

# Using Tomography Technique to Characterize the Continuous-Flow Mixing of Non-Newtonian Fluids in Stirred Vessels

Dineshkumar Patel, Farhad Ein-Mozaffari\*, Mehrab Mehrvar

Department of Chemical Engineering, Ryerson University  
 350 Victoria Street, Toronto, Ontario, M5B 2K3, Canada  
 fmozaffa@ryerson.ca

Chemical industries often encounter non-Newtonian fluids with yield stress such as pulp suspensions, certain polymer and biopolymer solutions, and wastewater sludge. The visualization of the non-Newtonian fluid flow inside the stirred vessels is a challenging task since the vast majority of these fluids are opaque. Electrical resistance tomography (ERT) is a non-invasive flow-visualization technique which can be utilized effectively for the evaluation of the mixing of opaque fluids. In this study, a cylindrical mixing vessel equipped with a top-entering impeller was employed to mix the xanthan gum solution, which is a pseudoplastic fluid exhibiting yield stress. The main objective of this study was to employ the ERT technique in the continuous-flow mixing of non-Newtonian fluid in order to explore: (i) the effect of the impeller type (radial-flow and close clearance impellers) on the flow pattern generated inside the stirred tank (ii) the effect of inlet-outlet flow on the deformation of the cavern. The 2D and 3D tomograms enabled us to visualize the flow of the opaque fluid and to identify the existence of channeling and dead volume inside the stirred vessel in the continuous-flow mixing system. Moreover, the tomography images revealed that the cavern volume increased due to the deformation created by the inlet-outlet flow.

## 1. Introduction

Owing to its vast applications, mixing is prevalent in several contexts of drinking water and wastewater treatment, food, and polymer processing. Chemical industries generally use non-Newtonian fluids with yield stress such as certain polymer and biopolymer solutions and wastewater sludge. Mixing of such fluids leads to the formation of a well-mixed region around the impeller (cavern) surrounded by a stagnant zone far from the impeller, where the shear stress is below the fluid yield stress. This condition in stirred vessels leads to non-ideal flows such as channeling, and dead volumes that radically affect the performance of the continuous-flow mixing of non-Newtonian fluids (Ein-Mozaffari et al., 2005). These non-ideal flows should be minimized in a vessel to improve the efficiency of the mixing system.

The effects of types of impeller (axial-flow, radial-flow, and close clearance), impeller off-bottom clearance, residence time, fluid height in the vessel, and jet velocity on the dynamic performance of continuous-flow mixing of non-Newtonian fluids were explored by Patel et al. (2011). They found that the extent of non-ideal flows such as channelling and dead volume decreased when the clearance of the impeller was increased from  $H/3.4$  to  $H/2.1$  (where  $H$  is the fluid height in a vessel) and the jet velocity was increased from  $0.317$  to  $1.66 \text{ m s}^{-1}$ . Furthermore, as the fluid height in the vessel was increased, the extent of non-ideal flows also increased while increasing the residence time of the fluid in the vessel decreased non-ideal flows. The performance of a continuous-flow mixing system depends on the fluid feed flow rate (Patel et al., 2012a) and fluid rheology (Ein-Mozaffari et al., 2007). The dynamic test results showed that the extent of non-ideal flows increased when the fluid yield stresses as well as the fluid flow rates were increased in the mixing of non-Newtonian fluids exhibiting yield stress (Patel et al., 2012b; Saeed and Ein-Mozaffari, 2008). Ein-Mozaffari et al. (2003) studied the effect of impeller size on the performance of continuous-flow mixing of non-Newtonian fluids with yield stress through dynamic tests. They observed

that the efficiency of the continuous-flow mixer improved as the impeller diameter was increased. Using CFD (Aubin et al., 2006; Khopkar et al., 2004), residence time distribution (RTD) (Samaras et al., 2006), laser Doppler velocimetry (LDV) (Mavros et al., 1997) and spectrophotometer (Roussinova and Kresta, 2008), some studies have also been carried out in the continuous-flow mixing of Newtonian-fluids in the stirred vessel and found that non-ideal flow such as channelling affect the performance of the mixing system. Newtonian fluids have been commonly used for the study of continuous-flow mixing in stirred tank reactors; however, a few studies have been carried out on the pseudoplastic fluids exhibiting yield stress. These studies have commonly identified non-ideal flows using dynamic tests, CFD, and RTD. Therefore, the aim of this study was to explore the effect of the inlet-outlet flow on the deformation of the cavern and to visualize flow patterns generated in the mixing of pseudoplastic fluids possessing yield stress in a stirred-tank reactor using 2D and 3D tomography images.

## 2. Experimental setup and procedure

In this study, we used the experimental set-up shown in Figure 1: (1) feed tank, (2) tracer tank, (3) metering pump, (4) solenoid valve, (5) progressive cavity pump, (6) electric motor, (7) torque meter, (8) mixing tank, (9) ERT data acquisition system, (10) electrode, (11) host computer, (12) discharge tank, (13) RT impeller (Rushton turbine), (14) Scaba impeller, (15) Maxblend impeller, (16) Inlet, and (17) Outlet. The mixing vessel consists of a transparent flat-bottomed cylindrical tank with a diameter ( $T$ ) of 0.38 m and a height of 0.60 m. The tank was equipped with four equally spaced baffles with a width of  $T/10$ . The fluid height ( $H$ ) in the tank was maintained at  $T/0.93$ . The diameters of the inlet and outlet pipes were  $T/15.2$ . The inlet was located at the top ( $r = 0.13$  m,  $\Phi = 90^\circ$ , and  $z = T$ ) and the outlet was located at the bottom ( $r = 0.13$  m,  $\Phi = 315^\circ$ , and  $z = 0/T$ ) of the mixing vessel. The fluid flow rate ( $Q$ ) was maintained at  $9.65$  L  $\text{min}^{-1}$ . The radial-flow impellers (RT and Scaba) with a  $T/2.1$  diameter ( $D$ ) and close clearance impeller (Maxblend) with a  $T/1.5$  diameter were utilized to mix the non-Newtonian fluids. The off-bottom clearance ( $C$ ) was set at  $T/2.4$ ,  $T/2.4$  and  $T/76$  for the Scaba, RT, and Maxblend impellers, respectively. Six tomography sensor planes were positioned around the circumference of the mixing tank. The planes were numbered from top ( $P1$ ) to bottom ( $P6$ ). The planes were 0.06 m apart from each other with the bottom plane 0.04 m from the bottom of the tank. Each plane had 16 stainless steel electrodes which were located equidistantly on the periphery of the vessel. The height, width, and thickness of the electrodes were 0.02, 0.03, and 0.001 m, respectively. Each electrode was in direct contact with the working fluid in the tank without invading the flow and was connected to the electrical resistance tomography (ERT) system (Industrial Tomography Systems, Manchester, UK). The tomography machine was connected to a computer for the image reconstruction. The mixing tank was equipped with a top-entering impeller driven by a 1.5 kW motor, and the impeller speed ( $N$ ) was set to the desired revolution per minute (rpm) using a variable frequency drive. The impeller speed was measured using a tachometer.

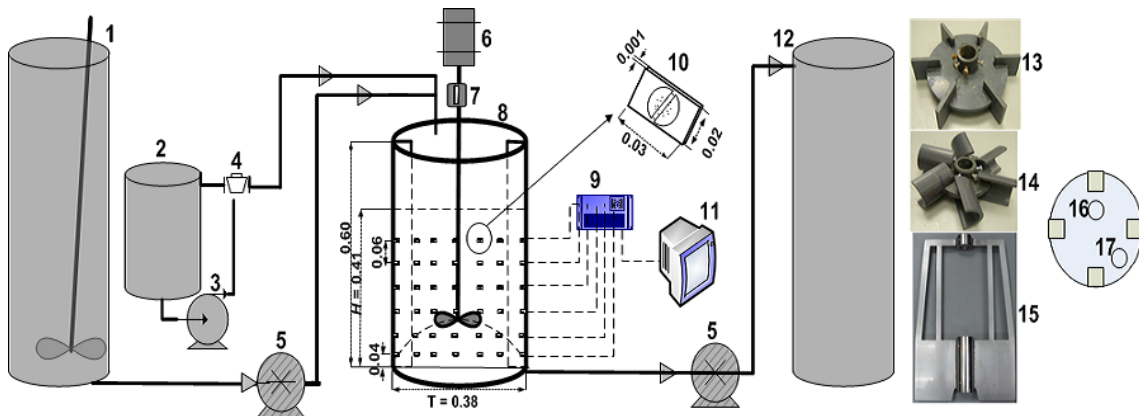


Figure 1: Experimental set-up (dimensions in m).

There were two procedures adopted: (i) to study the effect of the inlet-outlet flow on the deformation of the cavern and (ii) to visualize the flow pattern generated in the continuous-flow mixing. In the former procedure, 30 mL of 5 % saline solution (tracer) was injected near the impeller hub in the batch mode and the tracer concentration was monitored using ERT. Measurements were collected from six planes of electrodes until the cavern size remained unchanged. Once the cavern was fully developed in about 30 s,

the feed and discharge pumps were turned on simultaneously and the fluid was pumped from the feed tank to the discharge tank through the mixing vessel. ERT data were collected and tomography images were reconstructed to visualize the deformation of the cavern inside the mixing vessel. The cavern volume was calculated using the cavern diameter and the cavern height for a cylindrical shape.

While in the other procedure, the feed and discharge pumps were turned on simultaneously first and the fluid was pumped from the feed tank to the discharge tank through the mixing vessel. Then 150 mL of 9 % saline solution (tracer) was injected in the feed. Measurements were collected from six planes of electrodes. ERT data were collected and tomography images were reconstructed to visualize the distribution of the tracer concentration inside the mixing vessel. In both procedures, before the injection of the tracer, the reference state was taken to eliminate the effect of the stirrer and other internals within the mixing tank. In this study, the maximum concentration of the tracer in the solution was always below 0.17 %. The previous study (Saeed and Ein-Mozaffari, 2008) showed that the rheological properties of the xanthan gum solution did not change significantly when the tracer (NaCl) concentration in the tank was less than 0.17 %. In this study, xanthan gum powder was dissolved in water to prepare 1.0 % solution. Xanthan gum solution is a shear-thinning fluid possessing yield stress and its rheological properties can be described by the Herschel-Bulkley model (Herschel and Bulkley, 1926) ( $\Gamma = \Gamma_y + K (\zeta)^n$ , where  $\Gamma$  is the shear stress,  $\Gamma_y$  is the yield stress,  $K$  is the consistency index,  $\zeta$  is the shear rate, and  $n$  is the power-law index). The rheological properties of the xanthan gum solutions can be found in Saeed and Ein-Mozaffari, 2008.

ERT is used in the mixing of non-Newtonian fluids (Patel et al., 2013a,b). The ERT system consists of three main parts: sensing system, data acquisition, and image reconstruction. In the sensing system, the electrodes, fabricated from stainless steel, were used in this study. To make the electrical contact with the fluid inside the vessels, the electrodes were placed around the boundary of the vessel. These electrodes were connected to the data acquisition system (DAS). The adjacent strategy was used for image reconstruction. In this strategy, current is applied through a pair of two adjacent electrodes and voltages are measured at the remaining adjacent pairs of electrodes, and the injection pair is switched to the next pair of electrodes and repeated until all independent combinations are completed. Eventually, the DAS communicated these quantitative data to the host image reconstruction computer, where the data were processed using a suitable image reconstruction algorithm. The linear back projection algorithm (non-iterative) was used in this study.

### 3. Results and discussion

In this study, tomography was employed to visualize the deformation of the cavern by the input-output flow in the continuous-flow mixing system. As described in the procedure, once the cavern remained unchanged in the batch mode, the feed and discharge pumps were turned on at the same time. ERT data were collected and 2D tomography images were generated. These 2D images were obtained from planes  $P1$  to  $P6$  and were stacked to provide a snap shot at a certain time. Colors in tomograms show the distribution of the tracer in the vessel. The red color in the tomograms demonstrates the high-conductivity regions, and indicates the higher tracer concentration in those zones. The blue color shows the low-conductivity zones, and represents the lower tracer concentrations. 2D tomograms were converted into 3D images and were sliced using the Slicer Dicer software. Figure 2 shows the effects of the input-output flow on the deformation of the cavern for the Scaba impeller. These images are presented in five columns in a time series (1<sup>st</sup> column from left: 2D tomograms from planes  $P1$  to  $P6$ ; 2<sup>nd</sup> column: 2D images from planes  $P1$  to  $P6$  when the frames were stacked; 3<sup>rd</sup> column: Slicer Dicer block for the inverted position of the tank; 4<sup>th</sup> column: Slicer Dicer x-axis image; and the 5<sup>th</sup> column: Slicer Dicer y-axis image). In the 3<sup>rd</sup> column, the Slicer Dicer images of the tank are presented in an inverted position as it is difficult to view the bottom of the tank from the top. In this 3D image, the upper surface shows the bottom of the tank and the lower surface shows the top of the tank. The locations of the inlet and outlet are also shown in the Slicer Dicer images.

The ERT images depicted in the first row in Figures 2 were obtained at zero second (i.e. when the cavern size remained unchanged after the injection of the tracer in the batch mode and before the pumps were turned on). The images in the first row at zero second show that there was almost no tracer at the bottom plane  $P6$  in the 2D tomogram and the top surface of the inverted position of the tank. Once the feed and discharge pumps were started at the same time, images in the second row clearly showed that the cavern shape was slightly deformed at the bottom. This was due to the flow of fluid sucked from the bottom outlet ( $BO$ ) by the discharge pump. At that instant, the tracer appeared at plane  $P6$  in the 2D tomogram and the top surface of the inverted position of the tank. As the time passed, the fresh xanthan gum solution was continuously fed to the tank through the top inlet ( $T$ ) and the mixed solution was drawn from the vessel

through the bottom outlet (*BO*). Due to this input-output flow, the cavern shape recorded in the batch mode was deformed in the continuous mode. As times passed, the concentration of the tracer at the bottom plane *P6* in the 2D tomogram and the top surface of the inverted position of the tank increased as shown in the 3<sup>rd</sup> row image. It is clear from the images that the size of the cavern increased as the flow passed through the mixing tank. Finally, the cavern volume was increased by 11.0 % due to the deformation generated by the inlet-outlet flow. In fact, the momentum added to the fluid in the mixing vessel by the input-output flow resulted in the deformation of the cavern.

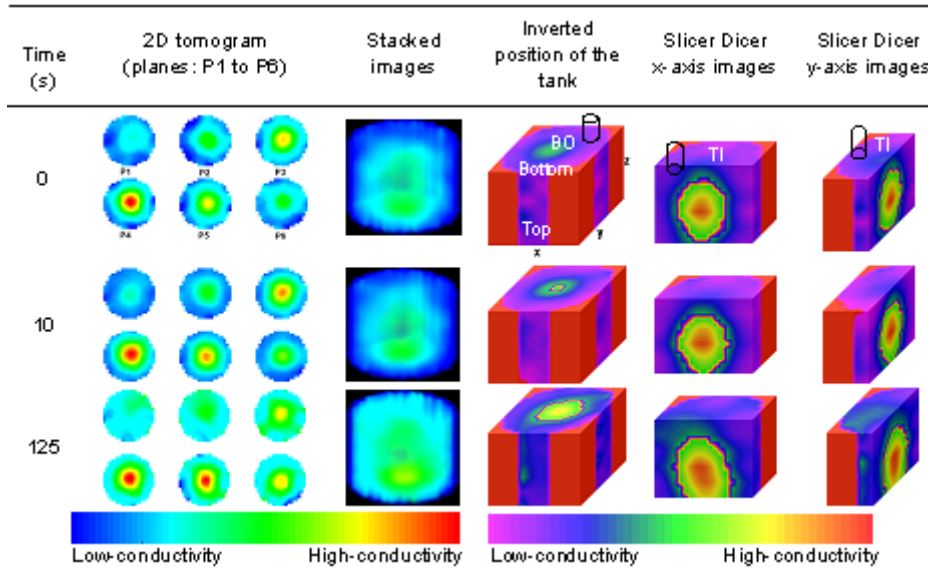


Figure 2: Effect of inlet-outlet flow on the deformation of the cavern for the Scaba impeller at  $N = 30$  rpm and 1 % xanthan gum solution.

The visualization of the tracer movement in continuous-flow mixing system is described below. As mentioned in the procedure, the feed and discharge pumps were turned on simultaneously and then the tracer was injected in the feed stream. ERT data were collected and tomography images were reconstructed to see the distribution of the tracer inside the mixing vessel. Figures 3 and 4 show the images generated in the mixing of 1 % xanthan gum solution for the RT impeller and for the Maxblend impeller, respectively. The ERT images in the first row (at zero second) in Figures 3 and 4 were obtained before the tracer injected into the feed stream. The blue color in tomograms shows that only xanthan gum solution was present and there was no tracer in the tank at that moment. In the second row, the color change in the ERT images shows that tracer was injected in the feed stream at the top of the vessel. It also shows that at that moment there was almost no tracer at the bottom plane *P6* in the 2D tomogram and the top surface of the inverted position of the tank. As time passed, the discharge pump withdrew the fluid from the bottom outlet (*BO*) and the tracer appeared at plane *P6* in the 2D tomogram and the top surface of the inverted position of the tank. The tomography images depicted in the Figure 4 show that the Maxblend impeller was capable of dispersing the tracer more effectively even at a lower impeller speed compared to the RT impeller. The Maxblend impeller consisted of a bottom paddle mounted by a top grid. The paddle was designed to generate flow circulation and the grid to provide capacity for dispersing a second phase (e.g. gas, liquid, or solid). These grids slowly assisted to disperse the tracer at the upper region of the tank. Moreover, the size of the Maxblend impeller was larger compared to the RT impeller. Thus, it swept higher volumes within the tank and provided a better mixing quality. Therefore, the dispersion of the tracer in the initial rows was much wider for the Maxblend impeller than for the RT impeller. The images in the last row show that the presence of paddle in the Maxblend impeller was effectively mixed the tracer at the bottom of the tank. Patel et al. (2012b) showed that the Maxblend impeller was the most effective amongst the Lightnin A320, Scaba 6SRGT, and anchor impellers for reducing the non-ideal flows in the continuous flow mixing of non-Newtonian fluid.

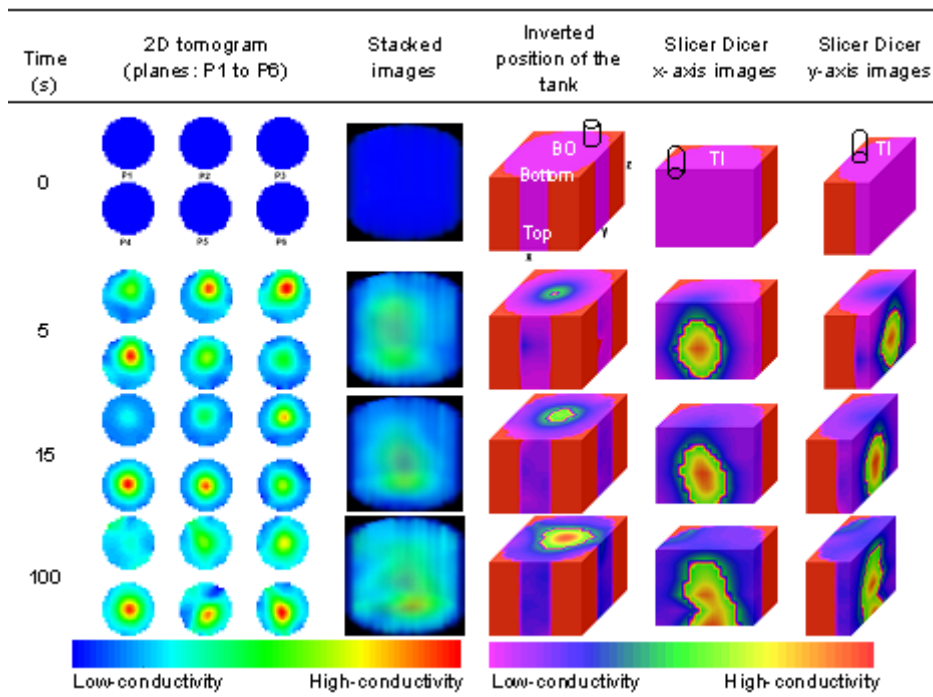


Figure 3: 2D and 3D images generated in the mixing of the 1 % xanthan gum solution for the RT impeller at 30 rpm.

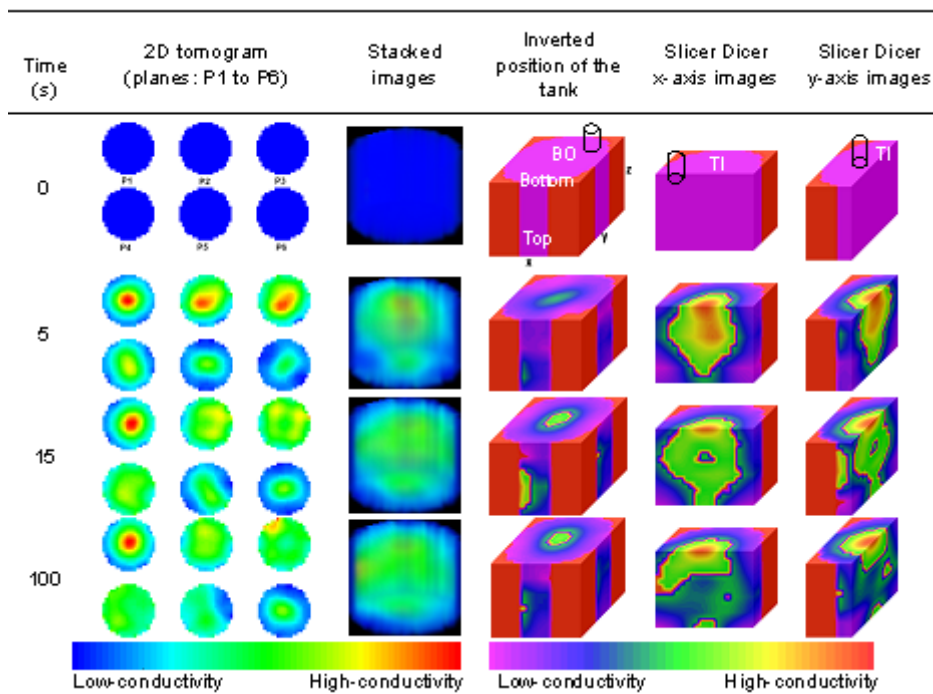


Figure 4: 2D and 3D images generated in the mixing of the 1 % xanthan gum solution for the Maxblend impeller at 25 rpm.

#### 4. Conclusions

Electrical resistance tomography (ERT) was utilized to visualize the flow of non-Newtonian fluids with yield stress in the continuous-flow mixing system. The effect of the input-output flow on the deformation of the cavern around the Scaba impeller was analyzed using the 2D and the 3D images. These results showed that the shape of the cavern was changed by inlet-outlet flow in the continuous-flow mixing system. ERT was also used to analyze the tracer distribution in the continuous-flow mixing of the non-Newtonian fluid for the RT and Maxblend impellers. This technique enabled us to successfully visualize how the tracer moved from the inlet to the outlet in the continuous-flow mixing system. Thus, the tomography images provided critical information regarding the mixing quality in the agitation of the opaque fluids.

#### Acknowledgements

The financial support of the Natural Science and Engineering Research Council of Canada (NSERC, PGS D2), Ontario Graduate Scholarship (OGS) and Ontario Graduate Scholarship in Science and Technology (OGSST) are gratefully acknowledged.

#### References

- Aubin J., Kresta, S.M., Bertrand J., Xuereb C., Fletcher D.F., 2006, Alternate operating methods for improving the performance of continuous stirred tank reactors, *Chem. Eng. Res. Des.* 84(A7), 569-582.
- Ein-Mozaffari F., Dumont G.A., Bennington C.P.J., 2003, Performance and design of agitated pulp stock chests, *Appita J.* 56(2), 127-133.
- Ein-Mozaffari F., Bennington C.P.J., Dumont G.A., 2005, Suspension yield stress and the dynamic response of agitated pulp chests, *Chem. Eng. Sci.* 60, 2399-2408.
- Ein-Mozaffari F., Bennington C.P.J., Dumont G.A., 2007, Optimization of rectangular pulp stock mixing chest dimensions using dynamic tests, *TAPPI J.* 6(2), 24-30.
- Herschel W.E., Bulkley R., 1926, Measurements of consistency as applied to rubber-benzene solutions, *Proc. Am. Soc. Test. Mat.* 26(2), 621-633.
- Khopkar A.R., Mavros P., Ranade V.V., Bertrand J., 2004, Simulation of flow generated by an axial flow impeller - batch and continuous operation, *Chem. Eng. Res. Des.* 82(A6), 737-751.
- Mavros P., Naude I., Xuereb C., Bertrand J., 1997, Laser Doppler velocimetry in agitated vessels: Effect of continuous liquid stream on flow patterns, *Chem. Eng. Res. Des.* 75(A), 763-776.
- Patel D., Ein-Mozaffari F., Mehrvar M., 2011, Dynamic performance of continuous-flow mixing of pseudoplastic fluids exhibiting yield stress in stirred reactors, *Ind. Eng. Chem. Res.* 50(15), 9377-9389.
- Patel D., Ein-Mozaffari F., Mehrvar M., 2012a, Effect of impeller type on continuous-flow mixing of non-Newtonian fluids in stirred vessels through dynamic tests, *Can. J. Chem. Eng.* 90(2), 290-298.
- Patel D., Ein-Mozaffari F., Mehrvar M., 2012b, Improving the dynamic performance of continuous-flow mixing of pseudoplastic fluids possessing yield stress using Maxblend impeller, *Chem. Eng. Res. Des.* 90(4), 514-523.
- Patel D., Ein-Mozaffari F., Mehrvar M., 2013a, Characterization of the continuous-flow mixing of non-Newtonian fluids using the ratio of residence time to batch mixing time, *Chem. Eng. Res. Des.* <http://dx.doi.org/10.1016/j.chemd.2013.01.013> (in press).
- Patel D., Ein-Mozaffari F., Mehrvar M., 2013b, Using tomography to characterize the mixing of non-Newtonian fluids with a Maxblend impeller, *Chem. Eng. Technol.* 36 (4), 687-695
- Roussinova V., Kresta S.M., 2008, Comparison of continuous blend time and residence time distribution models for a stirred tank, *Ind. Eng. Chem. Res.* 47(10), 3532-3539.
- Saeed S., Ein-Mozaffari F., 2008, Using dynamic tests to study the continuous mixing of xanthan gum solutions, *J. Chem. Technol. Biotechnol.* 83, 559-568.
- Samaras K, Mavros P, Zamboulis D., 2006, Effect of continuous stream and agitator type on CFSTR mixing state, *Ind. Eng. Chem. Res.* 45, 4805-4815.